

Article

A Kinetic Study on the Reduction of Single Magnetite Particle with Melting Products at High Temperature Based on Visual and Surface Analytical Techniques

Zhongjie Shen ¹ , Shuang Sun ¹, Yulong Zhu ¹, Dong Han ¹, Zhan Du ² and Haifeng Liu ^{1,*}

¹ School of Resources and Environmental Engineering, East China University of Science and Technology, Shanghai 200237, China; zjshen@ecust.edu.cn (Z.S.); y30180604@mail.ecust.edu.cn (S.S.); Y45180396@mail.ecust.edu.cn (Y.Z.); Y30140530@mail.ecust.edu.cn (D.H.)

² State Key Laboratory of Multiphase Complex Systems, Institute of Process Engineering, Chinese Academy of Sciences, Beijing 100190, China; zdu@ipe.ac.cn

* Correspondence: hfliu@ecust.edu.cn; Tel.: +86-21-64251418

Abstract: In this study, the reduction characteristics of single magnetite particles with melting products at high temperature were investigated by using visualization and surface analytical techniques. The morphology evolution, product type, reduction degree, and reduction rate of single magnetite particles during the reduction process were analyzed and compared at different reduction temperatures. The results showed that the morphology of the product formed at the reduction temperature of 1300 °C was a mainly nodular structure. When the reduction temperature was above 1400 °C, the products were melted to liquid and flowed out of the particle to form a layered structure. The morphology of the melted products finally transformed to be root-like in structure on the plate around the unmelted core. Raman spectroscopy was used to determine the product types during the reduction process. Experiments studying the effects of gas flowrate and particle size on the reduction degree were carried out, and the results showed that both increasing the temperature and gas flowrate can increase the reduction degree. The internal/external diffusion influence can be ignored with a particle size smaller than 100 μm and a gas flowrate more than 200 mL/min. However, owing to the resistance of the melted products to gas diffusion, the reduction rates at 1400 and 1500 °C were reduced significantly when the reduction degree increased from 0.5 to 1.0. Conversely, the formation of the liquid enlarged the contact area of the reducing gas and solid–liquid and further increased the reduction degree. The kinetics parameters, including average activation energy and pre-exponential factor, were calculated from the experimental data. The reduction kinetics equation of the single magnetite particle, considering the effect of melted products is also given in this study.



Citation: Shen, Z.; Sun, S.; Zhu, Y.; Han, D.; Du, Z.; Liu, H. A Kinetic Study on the Reduction of Single Magnetite Particle with Melting Products at High Temperature Based on Visual and Surface Analytical Techniques. *Metals* **2021**, *11*, 1268. <https://doi.org/10.3390/met11081268>

Academic Editors: Robert Bidulský, Jana Bidulská and Pasquale Cavaliere

Received: 7 June 2021

Accepted: 9 August 2021

Published: 11 August 2021

Publisher's Note: MDPI stays neutral with regard to jurisdictional claims in published maps and institutional affiliations.



Copyright: © 2021 by the authors. Licensee MDPI, Basel, Switzerland. This article is an open access article distributed under the terms and conditions of the Creative Commons Attribution (CC BY) license (<https://creativecommons.org/licenses/by/4.0/>).

Keywords: ironmaking; single magnetite particle; high-temperature reduction; melting product; reaction kinetics

1. Introduction

Ironmaking and steelmaking technologies are essential for the development of the infrastructure, industry, and economy of a country [1–3]. However, the traditional ironmaking technology, such as the blast furnace, consumes a great deal of energy and produces abundant carbon dioxide. To solve these issues, alternative and innovative ironmaking technologies have been developed, such as COREX, Midrex, FINEX, HIsarna, and flash ironmaking [4,5]. Among these, the novel flash ironmaking technology, which was conceived by Sohn et al. from the University of Utah, has received much attention in recent years [6–8]. This technology can omit the complicated procedures, remove the energy consumption of the coking and sintering processes, and improve energy efficiency.

A schematic diagram of the flash ironmaking process is given in Figure 1, for which the detailed information can be found in Ref. [8]. The flash ironmaking equipment mainly

includes a flash shaft, molten-iron bath, and uptake. This technology uses iron ore concentrates with a small particle size ($<100\ \mu\text{m}$), natural gas (CH_4), CO , H_2 , or mixed gases as raw materials. Solid and gas materials are injected from the top of the flash shaft. The fuel gas reacts with O_2 as partial oxidization, creating a reducing atmosphere and a high temperature zone between 1500 to 1800 K in the flash shaft. In the meantime, the iron ore concentrates are reduced at high temperature in this flash shaft, and they move downward to the molten-iron bath. The slag with light density will float on the molten iron and be discharged on one side of the furnace. Unreacted gases or gas products, such as CO_2 , CO , H_2 , and H_2O , etc., flow through the uptake to the heat exchanger and gas cleaning system. H_2 and CO in the exhausted gas will be sent back to the flash shaft as secondary utilization. In the molten-iron bath, CH_4 , H_2 , O_2 , and coal are injected for further reduction of unreduced iron oxides or to be oxidized for the potential combination of the subsequent steelmaking process.

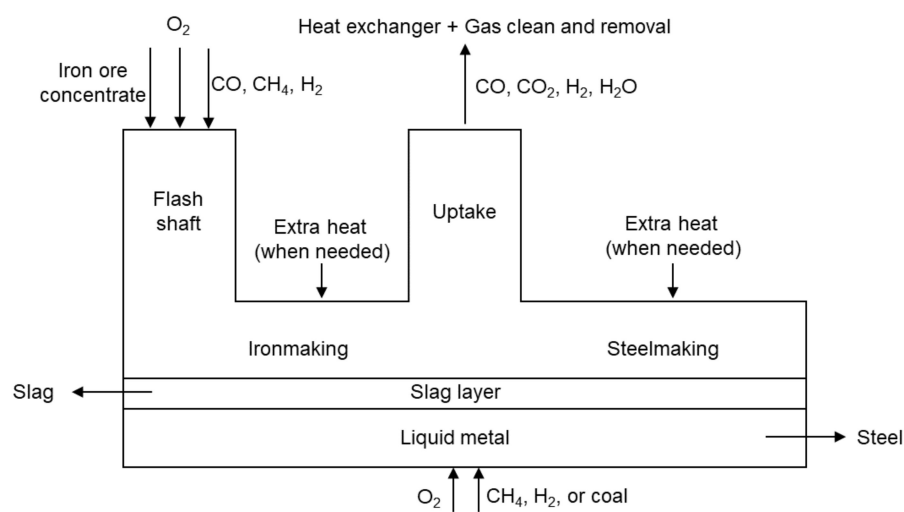


Figure 1. The schematic diagram of the flash ironmaking technology and its potential for the steelmaking process.

H_2 , CO , H_2O , and their mixtures are main gas reductants used in the alternative ironmaking technology and flash ironmaking technology [8–10], which can be produced from the gasification reaction with multiple solid fuels, such as coal or biomass [11,12]. Among these gases, H_2 is a highly reactive gas reductant for the reduction of iron ores. However, the disadvantage of this reduction is that it needs an extra external energy supply, which is commonly supplied from the combustion of CO , H_2 , and CH_4 with O_2 or the reduction of CO with Fe_2O_3 [8,13,14]. When the iron ore is reduced by the gas mixtures of H_2 and CO , the reduction rate of iron ore with H_2 is higher than the value in CO [10]. This causes the iron ore to react with H_2 first, decreasing the temperature of the reaction surface. Due to the low reduction reactivity of CO with iron ore, compared to H_2 , the extra heat supply from the reduction of iron ore with CO is not enough to hold the temperature, especially during the flash ironmaking process. Then, the reduction of iron ore with H_2 at lower temperature affects the total reduction rate of the iron ore. Thus, the following issue is the low reduction reactivity of CO with iron in the H_2/CO atmosphere [8,14]. The novel flash ironmaking technology operates at a high temperature around $1300\ ^\circ\text{C}$ and even close to $1400\ ^\circ\text{C}$ [8], and hence the reduction characteristics of iron ore in the mixing gases of H_2 and CO at high temperature are key to ensure both a sufficient heat supply for the reduction of H_2 with iron ore and to improve the overall reduction degree.

In the past, the reduction process from Fe_2O_3 to Fe above $570\ ^\circ\text{C}$ was considered to contain three steps: the initial step from Fe_2O_3 to Fe_3O_4 was a rapid reaction with the reduction degree from 0 to $1/9$ while the reduction degree of the secondary step from Fe_3O_4 to FeO ranged from $1/9$ to $1/3$ and the final step from FeO to Fe covered the degree

from 1/3 to 1.0 [6]. The reduction of hematite to magnetite has proved to be much faster than the other reduction steps. It was found that the reduction time of the step from Fe_3O_4 to FeO was faster than the step from FeO to Fe , nearly twice or more [9]. However, at high temperature, the other two steps from Fe_3O_4 to FeO and FeO to Fe were found to take place in parallel [9]. At high temperature, during the flash ironmaking process, it was found that Fe_2O_3 and FeO in the iron concentrates were mostly reduced to Fe within 1.2–7.7 s, occupying 95 wt.% of total iron particles [7]. In addition, it was found that the topochemical process from Fe_2O_3 to FeO was initially reaction-controlled [15,16]. Once a thin layer of iron oxides (magnetite or wüstite) formed on the surface during the reduction process, the rate-controlling of the reaction mechanism shifted to be diffusion-controlling [15]. Bohn et al. [17] carried out a study on the reduction kinetics of iron oxide in the gas mixtures of CO , CO_2 , and H_2 , and their results showed that the reduction from Fe_2O_3 to FeO , including two steps from Fe_2O_3 to Fe_3O_4 and Fe_3O_4 to FeO , was a first-order reaction in CO , and the reduction rate was controlled by intrinsic kinetics. Nevertheless, when the reduction temperature was higher than the melting points of the product, slag, or iron oxides, a liquid layer formed on the particle surface to cover the unreacted zone and hinder gas diffusion [18–20]. The melting behaviors of iron oxides or products have proved difficult to study for their intrinsic reduction kinetics. Li et al. [21] evaluated the effects of the temperature, gas composition ($\text{CO} + \text{H}_2$), and reduction degree on the sticking properties and found the sticking behavior of fresh iron with a high activity led to the rise of the sticking index at high temperature. Moreover, the high operating temperature during the flash ironmaking process causes melting and sticking behaviors of particles, significantly affecting the reduction process. Therefore, a further knowledge of the reaction characteristics of iron ore concentrates associated with melted products at high temperature is urgent to uncover the formation mechanism of the melting products and key to the kinetics study, which could help to optimize the novel flash ironmaking process.

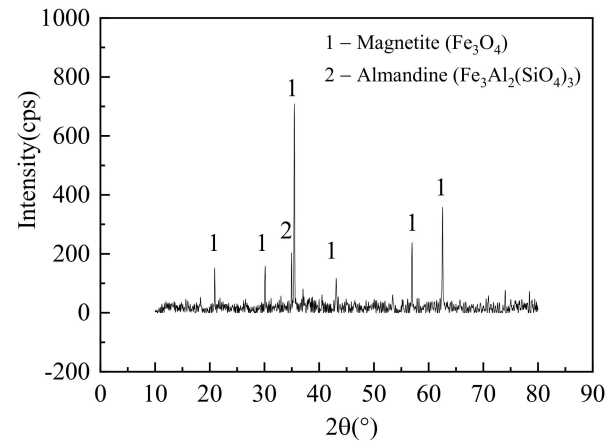
In this study, the reduction characteristics of a single magnetite particle with melting products at high temperature were investigated with visualization and surface analytical technique. The morphology evolution of single magnetite particles during the reduction process at different temperatures was recorded and analyzed by using a high temperature hot stage microscope (HTHSM). Raman spectroscopy was used to analyze and determine the type of the reduced product. Micromorphology and chemical composition were analyzed via scanning electron microscopy (SEM) with the combination of energy spectrum, respectively. The effects of reduction temperature, particle size and gas flowrate on the reduction degree were studied to determine the parameters of intrinsic kinetics. The activation energy and pre-exponential factor were calculated and compared with the model prediction. Finally, the reduction kinetics equation of magnetite particles at high temperature was given in this study.

2. Materials and Methods

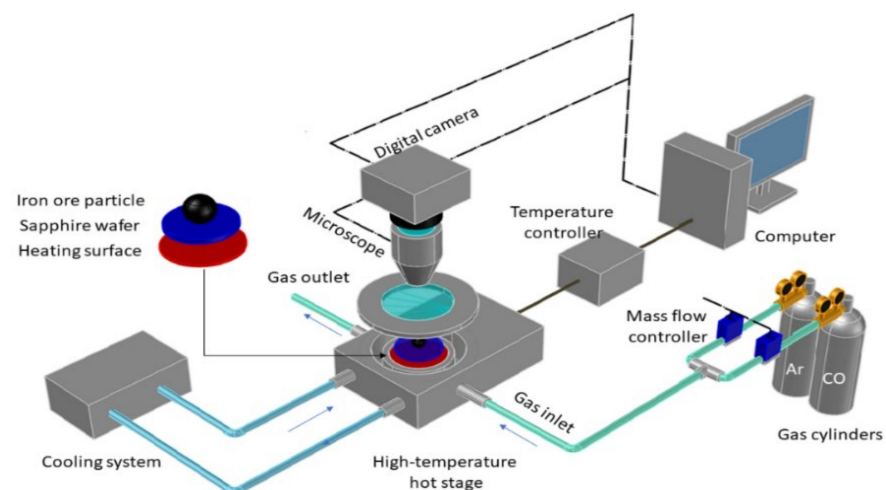
The magnetite sample from a Chinese ironmaking company was used as a raw material in this study. The sample was ground and screened to three size ranges (105–150 μm , 80–105 μm , and <80 μm). The screened samples were heated to 105 °C and held for 6 h to remove the moisture, and then were stored in the dryer with anhydrous silica gel particles. The chemical compositions of the magnetite sample were analyzed via an X-ray fluorescence spectrometer (XRF, ARL Advant'X Intellipower 3600, Thermo Fisher Scientific, Waltham, MA, USA) and are shown in Table 1. The mineralogical information of samples was analyzed by using a D/MAX 2550-VB/PC X-ray powder diffractometer (XRD, Malvern Panalytical B.V, Almelo, The Netherlands). The XRD analyzer used a Cu target and continuous scanning mode, and the diffraction angle of 2θ ranged from 10° to 80°. The XRD spectrum of the magnetite sample is given in Figure 2. The main phase was mainly magnetite (Fe_3O_4).

Table 1. Chemical composition of the raw iron ore sample.

Sample	Chemical Composition (wt.%)					
	Total Fe	SiO ₂	MgO	CaO	Al ₂ O ₃	Na ₂ O
Magnetite sample	65.40	6.07	1.24	1.15	0.79	0.43

**Figure 2.** XRD spectrum of the raw iron ore sample.

The reduction experiment of magnetite particles was carried out in a high temperature hot stage microscope (HTHSM), and the diagram of the experimental apparatus is shown in Figure 3. The high temperature hot stage microscope system included a DM4500P LED microscope with digital camera (Leica, Solms, Germany), a high temperature hot stage (Instec, MK2000, Boulder, CO, USA), gas transport system, cooling system and a computer. The temperature calibration before the experiment was carried out to ensure the accuracy of the setting temperature, with reference to the melting temperature of the silver (purity 99.9%). The relative error of the temperature calibration was controlled below 0.03% by repeating the experiments more than three times.

**Figure 3.** Schematic diagram of the high temperature hot stage microscope (HTHSM).

To study the reduction characteristics, magnetite particles on the sapphire wafer in the furnace of HTHSM were heated to different temperatures (1300, 1400, and 1500 °C) at the heating rate of 100 °C/min and held for 10 min to keep heat transfer balance. The furnace was sealed and an Ar gas flow (0.2 L/min, purity 99.999%) was injected as the purging gas to remove air inside. After 10 min, CO (purity 99.999%) was injected and replaced Ar as

the reactant gas. Meanwhile, the digital camera on the microscope recorded the reduction process automatically, including the reduction time and morphology evolution of magnetite particles. In this study, different CO gas flowrates and particle sizes were tested to study the effect of external and internal diffusion on the reduction. To determine the reduction degree at different reduction time, the gas flow of CO was injected and held for different time spots (e.g., 30 s, 45 s, 60 s, 75 s, 90 s and 120 s). The reduced magnetite particle was sealed via silicone oil after experiment to prevent being re-oxidized. Each experiment was carried out about 8–10 times to ensure the accuracy and reduce the measuring error. Furthermore, each experiment used 10 to 20 particles dispersedly distributed on the sapphire wafer.

After the experiment, Raman spectroscopy was used to analyze the type of the reduction products. The morphology and chemical composition of reduced magnetite particles were also analyzed by using the SV-1510 scanning electron microscope (Hitachi Company, Tokyo, Japan) combined with the energy spectrum (SEM-EDS).

The reduction degree from raw sample (Fe_3O_4) to metallic iron (Fe) was defined in terms of removable oxygen [22,23]

$$\alpha = \frac{m_0 - m_t}{m_0} = \frac{\Delta m}{m_0} \quad (1)$$

where Δm was the mass loss of oxygen during the reduction process, m_0 was the initial mass of oxygen and m_t was the mass of oxygen at time t . In this study, the raw material was magnetite. The reduction reaction from magnetite to metallic Fe followed two steps as $\text{Fe}_3\text{O}_4 \rightarrow \text{FeO} \rightarrow \text{Fe}$.



According to the mass conservation of Fe during the reduction process, the mass ratio of O to Fe was set as the variable and denoted as:

$$x = \frac{m_{\text{O}}}{m_{\text{Fe}}} \quad (2)$$

The initial mass fraction ratio of O to Fe from energy spectrum was about $x_0 = 0.4013$ while $x_m = 0.381$ in magnetite. The ratio of Fe to O measured from EDS has errors due to the surface detection. The mass loss of oxygen during the reduction from magnetite to metallic iron was two thirds of the measured mass loss both in reaction (R1) and reaction (R2). Therefore, this detection of the ratio of O to Fe was repeated two or three times for given error bars. The mass of oxygen in the impurities, such as SiO_2 , MgO , CaO , Al_2O_3 and Na_2O , needed to be removed from the calculation. Therefore, the reduction degree (α) in this study could be denoted as:

$$\alpha = \frac{\Delta m}{m_0} = 1 - \frac{x - (x_0 - x_m)}{x_m} = \frac{x_0 - x}{x_m} \quad (3)$$

3. Results

3.1. Single Particle Reduction Process

The reduction processes of the magnetite particles at different temperatures in CO atmosphere are shown in Figure 4. The results showed that the total reduction time of a single magnetite particle was about 90 s at 1500 °C while this time at 1300 and 1400 °C was 210 and 150 s, respectively. This indicated that the increase of the reduction temperature would produce benefit by reducing the reduction time. At 1300 °C, metallic bright spots were found on the particle surface, and these spots were missing at 1400 and 1500 °C. At both 1400 and 1500 °C, part of the reduction products was melted to liquid and flowed out of the particle to form a layered structure on the sapphire wafer. Root-like metallic luster substances appeared on the surface around the solid particle. The proportion of the area of the melted product to the observation field increased with the reduction time and

temperature, indicating that more products were melted to liquid at a higher temperature. Therefore, during the high-temperature reduction process of a single magnetite particle, a layered structure appeared around the particle, which is like an “egg”, accompanied by the reduction of the molten layer and the simultaneous reduction of central solid parts.

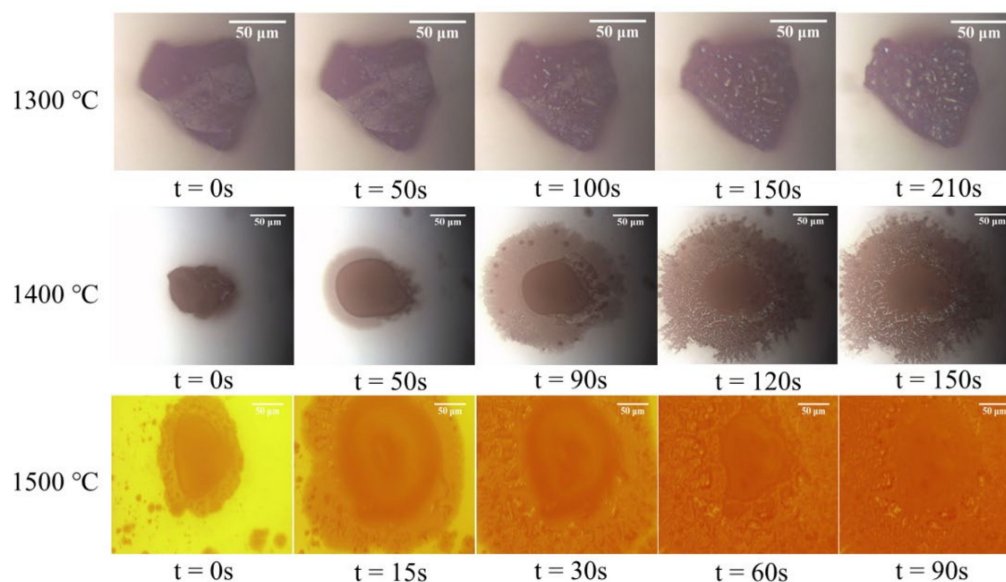


Figure 4. Images of reduction processes of single magnetite particle in the CO atmosphere at different temperatures.

3.2. Raman Analysis

The magnetite particle before/during/after the reduction process was analyzed by Raman spectroscopy (DXR™ Raman Spectroscopy, Thermo Fisher Scientific, Waltham, MA, USA) to determine the product type. The Raman spectra of the analyzed samples are shown in Figure 5. The standard Raman shifts of iron oxides are also given in Table 2. Compared to standard Raman shifts in Table 2, the raw sample, namely the magnetite particle, before reduction was mainly Fe_3O_4 , corresponding to the results of XRD spectrum in Figure 2. The Raman shifts of the raw sample tested in this study were 301, 534, and 663 cm^{-1} , which were same as the data from the literature [24,25]. Moreover, less Fe_2O_3 was found from the Raman spectra in Figure 5, corresponding to 227 cm^{-1} . Although the silicone oil could seal the product, fewer reduction products detected from the Raman spectroscopy were not completely similar with the standard shifts of FeO, and FeO was not stable and easily transformed as Fe_2O_3 or Fe_3O_4 . After the magnetite particle was reduced by CO at 30 s, two peaks corresponding to the Raman shifts of 616 and 663 cm^{-1} [24,25] were found in the tested samples at 1300 and 1400 °C, respectively. This indicated that magnetite was reduced to wüstite within a short time, about 30 s. When the reduction temperature was 1500 °C, more peaks were found in the spectrum, such as 435, 616, and 663 cm^{-1} . The higher temperature benefited the reduction from Fe_3O_4 to FeO. When the reduction was completed, the Raman spectra of samples showing a line without peaks was shown in Figure 5. Therefore, it was verified that the single particle was fully reduced to Fe after the experiment in HTTSM. The main controlling step was the reaction (R2) with the lower reaction rate from FeO to Fe.

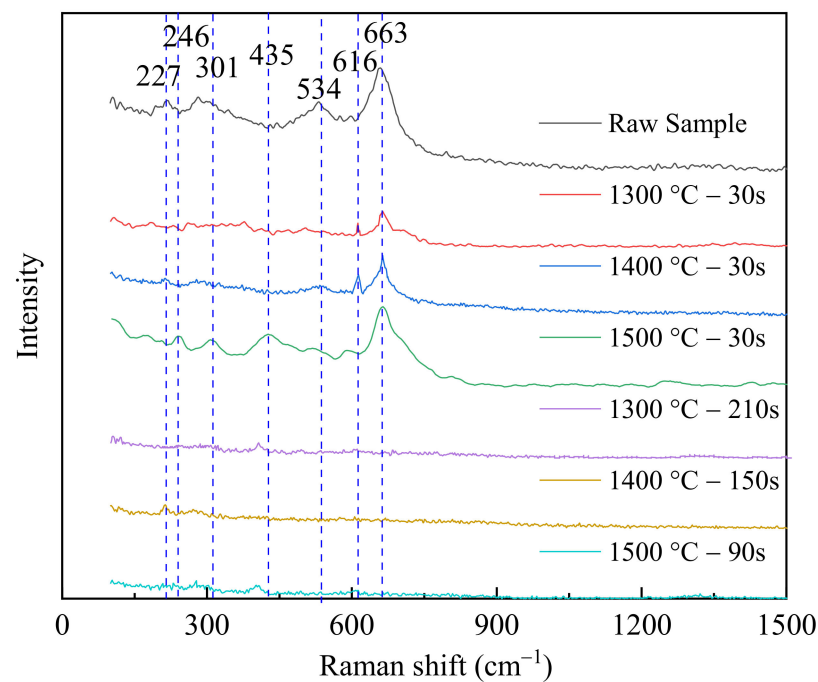


Figure 5. Raman spectra of samples before/during/after the reduction process.

Table 2. Raman shifts of different iron oxides [24,25].

Components	Raman Shift/cm ⁻¹						
α -Fe ₂ O ₃	227	246	293	411	497	612	1320
Fe ₃ O ₄	301.6	513	533.6	616	663		
FeO		435	616	663			
γ -FeOOH	252	380	526	650	1307		

3.3. Particle Morphologies

Figure 6 gives the SEM images and experimental photos of the particle morphology before/during/after the reduction process at different temperatures (1300, 1400 and 1500 °C). The times after the temperature means the reduction time of the particle. Photos on the right column are captured from HTHSM with 20 μ m bar scale. Here, at the same experimental temperature, the particle in the SEM image on the same line was not the same because the partially reduced particle would be oxidized after SEM analysis and then morphology would be changed. Therefore, particles were selected at 30 s and those with complete reduction for analysis. Their experimental conditions were the same, and only the reduction time was different. Basically, a magnetite particle has a smooth surface in the SEM image. Fine particles on this surface are caused by the magnetism property. When the reduction temperature was 1300 °C, a nodular structure occurred on the particle surface at 30 s. At this temperature, the magnetite particle was not melted. After the reduction process, the bulk of the nodular structures were found and formed on the surface. When the reduction temperature increased to 1400 °C, the proportion of the number of nodular structures decreased and part of the reduction products was melted, displaying a layered structure in the SEM image. The nodular structure was still found on the particle surface at 30 s but melted products formed and flowed around the particle onto the sapphire wafer. After the reduction process, the central part of the particle was solid with a nodular structure on the surface, and the external layer was mainly the surrounding molten product. At 1500 °C, no nodular structure was found on the particle surface when the reduction time was 30 s. The central part performed as a smooth surface of the particle with a root-like structure of melted products surrounding it. When the reduction was completed, a layered structure was shown in the SEM image, and the product was melted. Therefore, by

increasing the reduction temperature, the nodular structure formed on the particle surface at a low reduction temperature would be changed to a root-like structure and flow out around the central particle. The morphology evolution of the magnetite particle during the high temperature reduction process indicated that the reduced product or slag were melted and might cause reaction resistance for the further reduction.

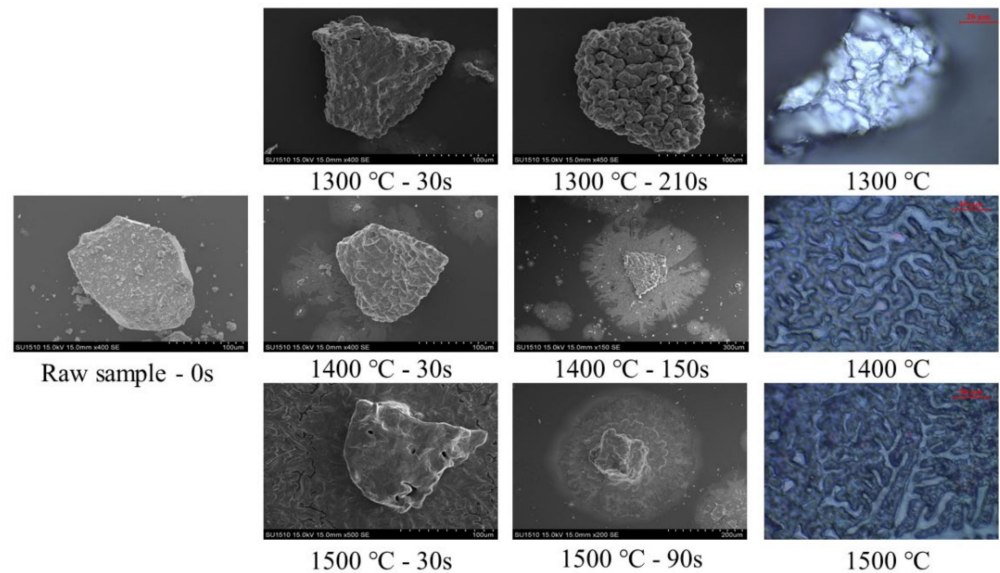


Figure 6. SEM images and experimental photos of particles before/during/after the reduction process at different temperatures.

4. Discussion

4.1. Effect of Gas Flowrate

The effect of gas flowrate on the reduction of magnetite particles was studied and the results are shown in Figure 7. The operating temperature was set to 1500 °C. The magnetite samples were reduced within different time frames (30, 45, 60, 75 and 90 s) to calculate the evolution of the reduction degree. Then, the mass fraction ratio of O to Fe was detected by energy spectrum and calculated from Equation (2). Error bars are also given in Figure 7. The gas flowrate ranged from 50 to 300 mL/min. The reduction degree increased with the increasing gas flowrate from 50 to 200 mL/min. When the gas flowrate was above 200 mL/min, the reduction degree at each tested time point did not change much from 200 to 300 mL/min. This indicated that the external diffusion effect on the reaction was minimized when the gas flowrate was above 200 mL/min. To ensure the minimized external diffusion effect, a gas flowrate of 250 mL/min was chosen in this study. Compared to the results from the study of Chen et al. [26], the external diffusion effect on the reduction of iron ore fines could be removed when the gas flowrate was 300 mL/min. Their experimental temperature was set to 700 °C. In this study, the temperature was much higher than the value in the literature [26], and the increasing reduction temperature also enhanced the diffusion of gas diffusion from the ambient phase to the particle surface, causing diffusion to proceed more quickly.

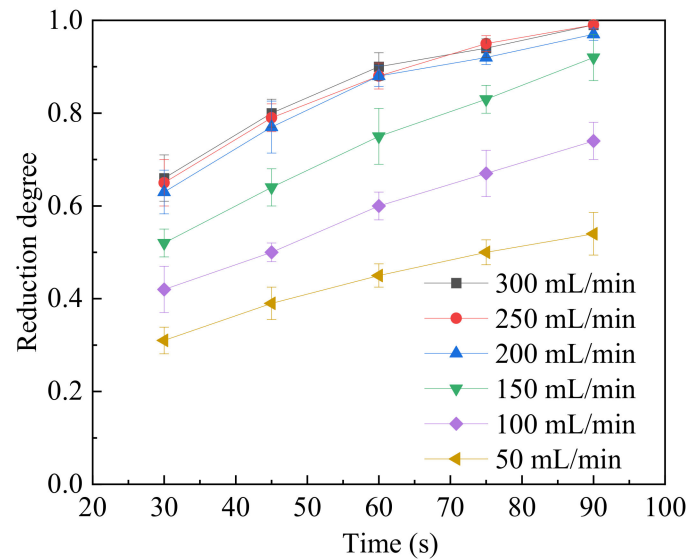


Figure 7. The relationship between the reduction degree and reduction time under different gas flowrates.

4.2. Effect of Particle Size

The study on the effect of different particle sizes on the reduction degree of the magnetite particles was carried out, and the results are shown in Figure 8. The gas flowrate was set at 250 mL/min herein, minimizing the effect of external diffusion, and the time spots for the measurement were also set as 30, 45, 60, 75 and 90 s. The operating temperature was set to 1500 °C. Results calculated from Equation (2) showed that the reduction degree increased with the decrease of the initial particle size. For the fine magnetite particle (<80 μm or 80~105 μm), the reduction degree displayed a similar tendency. However, when the particle size increased from 105 to 150 μm, the reduction degree decreased obviously. Large particles have a longer diffusion path for gas than fine particles, resulting in the reduction of the magnetite particles with larger particle size (>105 μm) being controlled by the internal diffusion of the reactant gas. Furthermore, at high temperatures, the reduced product or slag were melted and hindered the reducing gas diffusing into the internal zone of the particle, especially for the coarse particles.

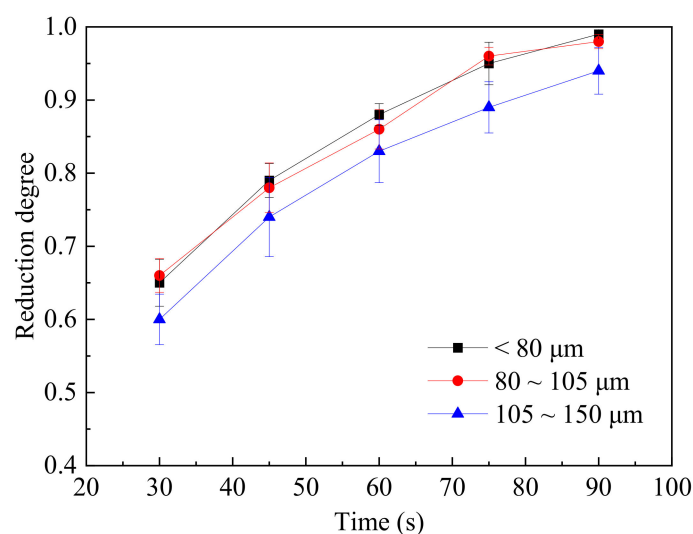


Figure 8. The relationship between the reduction degree and reduction time at different particle sizes.

4.3. Effect of Reduction Temperature

To study the effect of temperature on the reduction degree, the magnetite particles with size of 80 μm and gas flowrate of 250 mL/min were chosen in this study. According to the results from the previous sections, the internal/external diffusion effects were minimized. The results of the reduction degree at different temperatures from 1300 to 1500 $^{\circ}\text{C}$ were calculated and are shown in Figure 9. The reduction reaction was controlled by the chemical reaction under this condition. From Figure 9, with increasing temperature, the reduction degree increased obviously from 1300 to 1500 $^{\circ}\text{C}$. At 1500 $^{\circ}\text{C}$, the total reduction time was about 90 s while the reduction time at 1300 and 1400 $^{\circ}\text{C}$ was prolonged to 150 s and 210 s, respectively. High temperature benefited the reduction of magnetite and reduced the reduction time from the results in Figure 9. Additionally, the formation of a melted surface increased the contact area with the gas, which promoted the reaction.

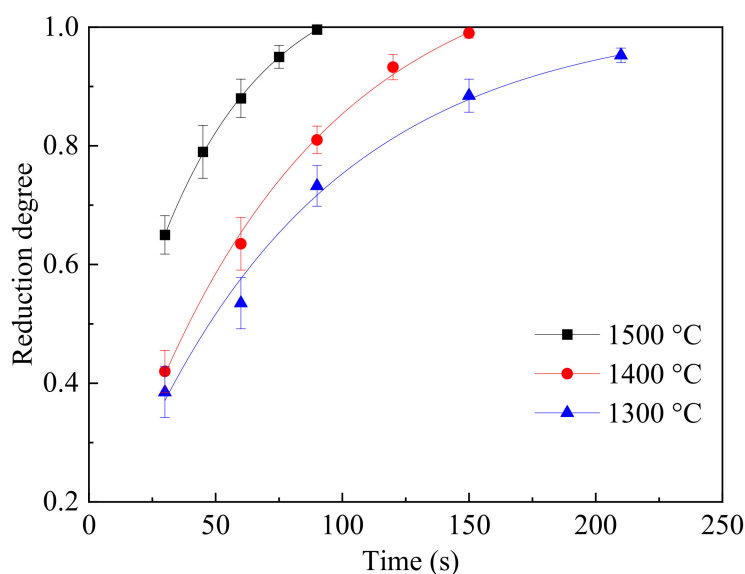


Figure 9. The relationship between the reduction degree and reduction time at different temperatures.

The relationship of the reduction rate and reduction degree at different temperatures is given in Figure 10. At 1300 $^{\circ}\text{C}$, the reduction rate first increased and then decreased rapidly with the reduction degree. At 1400 and 1500 $^{\circ}\text{C}$, the reduction rates decreased with the increasing reduction degree. The results also showed that the correlation parameters (R') at high temperature (1400 and 1500 $^{\circ}\text{C}$), which were 0.9804 and 0.9974, respectively, were higher than the value at 1300 $^{\circ}\text{C}$. This indicated that the reduction rate was dramatically decreased when the particle reached a high reduction degree at high temperature. When the reduction temperature was 1300 $^{\circ}\text{C}$, the reduction rate first increased and then decreased with the increasing reduction degree. This change was caused by the state of the reduction products, transforming from a solid to liquid, which was wüstite in this study. When the temperature was lower than the melting points of slag or product, the magnetite sample was solid at 1300 $^{\circ}\text{C}$. Owing to the heat from the reduction of FeO with CO, the particle temperature increased and resulted in the melting behavior of the reduction products. The resistance of gas diffusion to the inner layer was enlarged. The rate controlling was changed from a surface reaction to gas diffusion. During the reduction, once a thin layer of lower iron oxides (wüstite in this study) was formed on the particle surface, the reaction mechanism shifted to diffusion control [15]. The increasing reduction temperature also promoted the initial reaction from Fe_3O_4 to FeO. With this, the melted product or slag at high temperature decreases the reduction rate. The diffusion was rate controlling at this temperature and reaction stage.

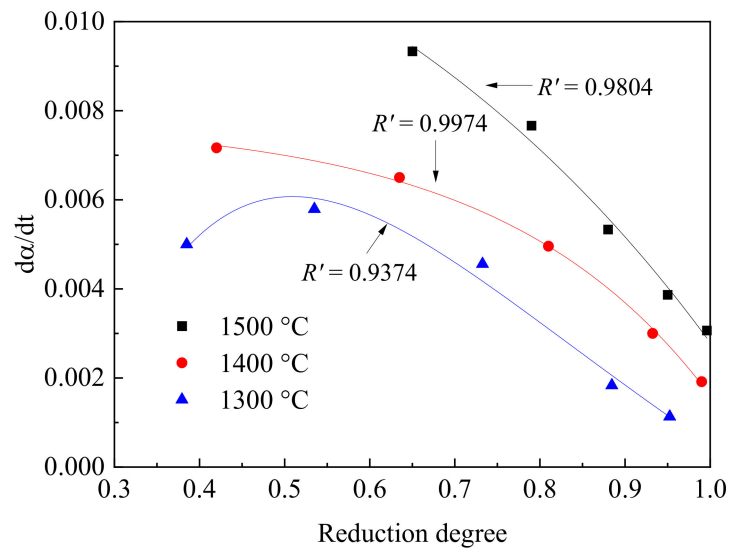


Figure 10. The relationship of reduction rate ($d\alpha/dt$) and reduction degree at different temperatures. R' denotes the correlation degree.

4.4. Parameters of Reaction Kinetics

The mass loss of O in the reaction (R1) was less than reaction (R2) with a higher reaction shift coefficient. The aim of this study was to investigate the reaction kinetics of the reaction (R2) from FeO to O, which was the controlling step in the total reduction reaction. The reduction reaction of magnetite with CO was a gas–solid reaction, and based on the general kinetic equation, the reaction rate could be written as [27–29]:

$$\frac{d\alpha}{dt} = k(T)f(\alpha) \quad (4)$$

where $f(\alpha)$ was the function of the reaction mechanism, and $k(T)$ was the reaction rate coefficient. t was the reaction time and T was the temperature.

According to the Arrhenius's Equation, the reaction rate coefficient was given as:

$$k(T) = Ae^{-E/(RT)} \quad (5)$$

Taking the natural logarithm of both sides of Equation (4) leads to

$$\ln \frac{d\alpha}{dt} = -\frac{E}{RT} + \ln A + \ln f(\alpha) \quad (6)$$

The activation energy (E) could be calculated from the relationship line of $\ln(d\alpha/dt)$ and $1/T$. The natural logarithm of the reduction rate at the degree nodes from 0.65 to 0.91 from Figure 10 was calculated and the linear equation between $\ln(d\alpha/dt)$ and $1/T$ is given in Figure 11. Then the slope of the line could be calculated. The activation energy was calculated from the multiplier of the slope and universal gas constant (-8.3145×10^{-3} kJ/mol), which is given in Table 3. The average activation energy was 109.6 kJ/mol. It could be found that the activation energy increased with the reduction degree, indicating the surface reaction energy barrier increased gradually, the reaction resistance increased while the reaction rate decreased. A weak correlation was found when the reduction degree was above 0.95. This indicated that there was something that limited the fitting for the reaction approaching to the stage with a high reduction degree. This linear difference was mainly caused by the covered raw material that could not be reduced. At 1300 °C, the final product acted as a particle, which differed from the products at 1400 and 1500 °C. This results in the liquid layer inside the particle covering the inner part, and the reducing gas cannot diffuse to this layer. In contrast, the reduced products were melted to liquid at 1400 and 1500 °C

and flowed out of the particle to the sapphire wafer. The inner, unreacted magnetite was exposed and could continue to react with the reducing gas, giving the high reduction degree in Figure 9. However, the liquid layer still reduced the gas diffusion rate, as shown in Figure 10. Therefore, the resistance from the liquid product for the gas diffusion caused the different reduction degree at different temperatures and the further difference for the fitting results.

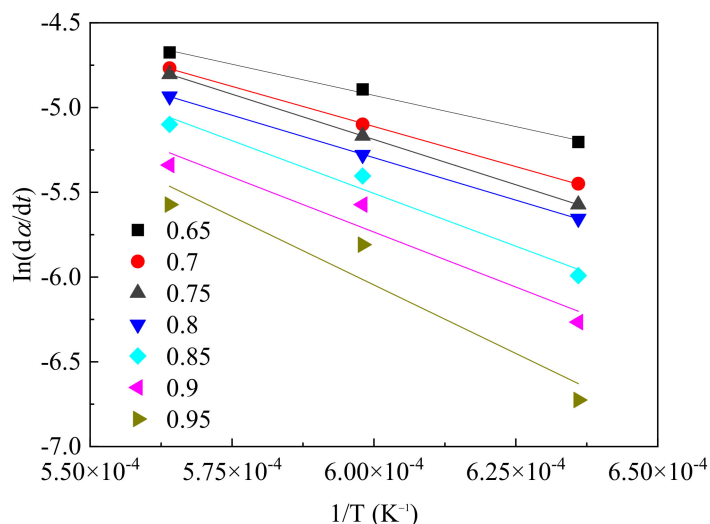


Figure 11. $\ln(da/dt)$ versus $1/T$ at different reduction degrees.

Table 3. Activation energy at different reduction degrees.

Reduction Degree	0.65	0.70	0.75	0.80	0.85	0.90	0.95	Average
Activation energy (kJ/mol)	61.16	78.65	88.82	83.28	103.5	107.9	134.4	109.6

In this study, the mechanism function $f(\alpha)$ and pre-exponential factor (A) were matched from models and experimental data in the literature [28]. According to the gas–solid model, the integration of the model equation yields [28]

$$G(\alpha) = k(T) \times t \quad (7)$$

Then the reaction rate coefficient and mechanism could be given from the linear fitting of $G(\alpha)$ and t . $k(T)$ was the slope of the line. The activation energy (E) and pre-exponential factor (A) could be calculated from the graph of $\ln k(T)$ and $1/T$.

According to the results, the external/internal diffusion effect on the reaction was removed by controlling the gas flowrate and particle size. Therefore, the total reaction was controlled by the chemical reaction kinetics. The reaction was assumed as a first-order reaction and $G(\alpha) = -\ln(1 - \alpha)$ [30]. The linear fitting at three different temperatures is given in Figure 12 and the degree of fitting (R^2) was 0.9758, 0.9793 and 0.9931, respectively, which proved the availability of the model in this study.

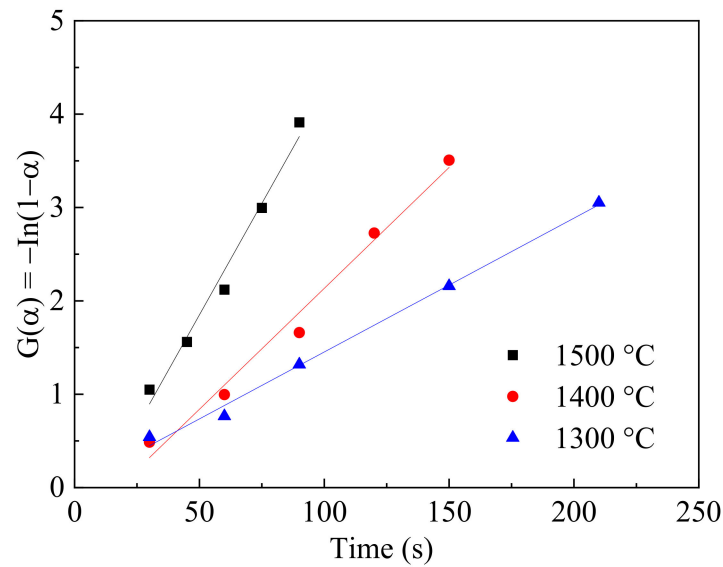


Figure 12. Linear fitting of $G(\alpha)$ and time at different temperatures.

$\ln k(T)$ was obtained from the natural logarithm of the slope of the fitting line from Figure 12. The activation energy and pre-exponential factor could be made from the fitting line of the $\ln k(T)$ and $1/T$, which is shown in Figure 13. The activation energy (E) was about 103.3 kJ/mol and the pre-exponential factor (A) was 38.86 s^{-1} , which showed good agreements with the results of Arrhenius Equation. Fan et al. [31] reported the activation energy was about 451 kJ/mol from 1200 to 1350 °C and 88 kJ/mol from 1350 to 1600 °C from Fe_3O_4 to Fe, while Jozwiak et al. [32] reported the activation energy about 104 kJ/mol for reaction (R2). Compared to the data from this literature [31,32], the results in this study were smaller because the resistance of melted products was not considered before. The reduction process of the single magnetite particle was conducted with melting behaviors generally happening at a high temperature and cannot be ignored. Thus, it is proved the accuracy of the calculation method and the applicability of the research method in this study. Finally, the reaction kinetics equation of magnetite during reduction at high temperature from FeO to O with effect of melted products could be denoted as:

$$\frac{d\alpha}{dt} = 38.86 \times (1 - \alpha)e^{-103.3 \times 1000 / (8.314T)} = 38.86 \times (1 - \alpha)e^{-1.242 \times 10^4 / T} \quad (8)$$

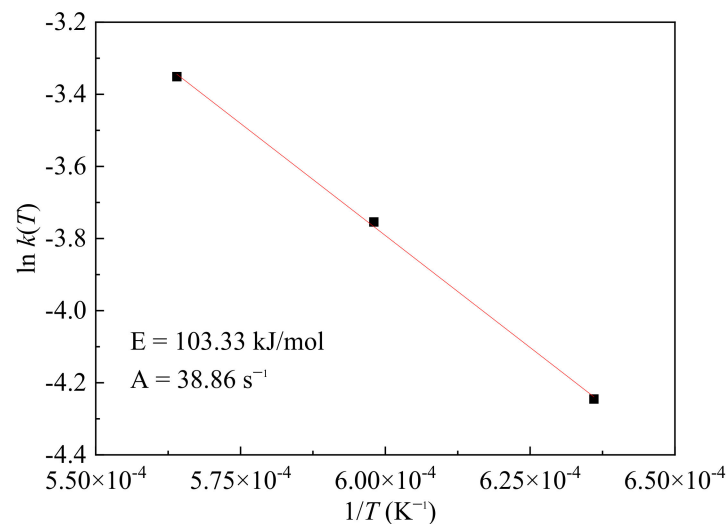


Figure 13. Linear fitting of $\ln k(T)$ and $1/T$.

5. Conclusions

The reduction characteristics of single magnetite particles with melting products at high temperature were investigated via visualization and surface analytical techniques. From the in situ experiments, particle morphology and its evolution during the reduction process were obtained and analyzed. The results showed that the melting behavior of the product or slag were found around the particle when the reduction temperature increased from 1300 to 1500 °C. At 1300 °C, the morphology of the reduction product mainly was a nodular structure on the particle surface. This structure transformed to a root-like structure at a higher temperature, attributed to the melting behavior of the product or midrate product during the reduction process. For the reduction of single magnetite particles, a gas flowrate higher than 200 mL/min and a particle size smaller than 100 µm were suitable conditions to study the intrinsic kinetics with minimized external and internal diffusion influences. The reduction rate at 1300 °C first increased and then decreased while at a higher temperature (>1400 °C) this rate decreased obviously due to the resistance of the melting products or slag to gas diffusion. A good finding of the study was that the reduction degree still increased with the reduction temperature. The subsequent reduction from FeO to Fe presented as the controlling process in the total reduction reaction. The average activation energy of the reduction of magnetite was proposed at about 109.62 kJ/mol. With the model matching method, the calculated activation energy was about $E = 103.33$ kJ/mol and the pre-exponential factor was 38.86 s⁻¹. The reduction kinetics equation (FeO → Fe) with the effect of melted products is also given in this study.

Author Contributions: Conceptualization, Z.S. and H.L.; methodology, Z.S. and D.H.; formal analysis, Z.S.; investigation, Z.S., D.H., S.S. and Y.Z.; resources, Z.S.; data curation, D.H. and Z.S.; writing—original draft preparation, Z.S.; writing—review and editing, Z.S., Z.D. and H.L.; supervision, H.L.; project administration, Z.S., Z.D. and H.L. All authors have read and agreed to the published version of the manuscript.

Funding: This study was funded by the National Natural Science Foundation of China (Grant No.21908063), and the Open Research Fund of State Key Laboratory of Multiphase Complex Systems (No. MPCS-2021-D-07).

Institutional Review Board Statement: Not applicable.

Informed Consent Statement: Not applicable.

Data Availability Statement: Not applicable.

Conflicts of Interest: The authors declare no conflict of interest.

References

1. Zhao, J.; Zuo, H.B.; Wang, Y.J.; Wang, J.S.; Xue, Q.G. Review of green and low-carbon ironmaking technology. *Ironmak. Steelmak.* **2020**, *47*, 296–306. [[CrossRef](#)]
2. Wang, Y.J.; Zuo, H.B.; Zhao, J. Recent progress and development of ironmaking in China as of 2019: An overview. *Ironmak. Steelmak.* **2020**, *47*, 640–649. [[CrossRef](#)]
3. Naito, M.; Takeda, K.; Matsui, Y. Ironmaking technology for the last 100 years: Development to advanced technologies from introduction of technological know-how, and evolution to next-generation process. *ISIJ Int.* **2015**, *55*, 7–35. [[CrossRef](#)]
4. Anameric, B.; Kawatra, S. Direct iron smelting reduction processes. *Miner. Process. Extr. Metall. Rev.* **2009**, *30*, 1–51. [[CrossRef](#)]
5. Qu, Y.X.; Yang, Y.X.; Zou, Z.S.; Zeilstra, C.; Meijer, K.; Boom, R. Thermal decomposition behaviour of fine iron ore particles. *ISIJ Int.* **2014**, *54*, 2196–2205. [[CrossRef](#)]
6. Chen, F.; Mohassab, Y.; Zhang, S.Q.; Sohn, Y. Kinetics of the reduction of hematite concentrate particles by carbon monoxide relevant to a novel flash ironmaking process. *Metall. Mater. Trans. B.* **2015**, *46*, 1716–1728. [[CrossRef](#)]
7. Chen, B.J.; Xiong, J.; Li, M.; Feng, Y.; Hou, W.Y.; Li, H.S. Numerical Investigation into Gas-Particle Inter-Phase Combustion and Reduction in the Flash Ironmaking Process. *Metals* **2020**, *10*, 711. [[CrossRef](#)]
8. Sohn, H.Y.; Fan, D.Q.; Abdelghany, A. Design of novel flash ironmaking reactors for greatly reduced energy consumption and CO₂ emissions. *Metals* **2021**, *11*, 332. [[CrossRef](#)]
9. Chen, H.S.; Zheng, Z.; Chen, Z.W.; Bi, X.T. Reduction of hematite (Fe₂O₃) to metallic iron (Fe) by CO in a micro fluidized bed reaction analyzer: A multistep kinetic study. *Powder Technol.* **2017**, *316*, 410–420. [[CrossRef](#)]

10. Kim, W.H.; Lee, S.; Kim, S.M.; Min, D.J. The retardation kinetics of magnetite reduction using H₂ and H₂-H₂O mixtures. *Int. J. Hydrog. Energy* **2013**, *38*, 4194–4200. [[CrossRef](#)]
11. Guo, D.B.; Zhu, L.D.; Guo, S.; Cui, B.H.; Luo, S.P.; Laghari, M.; Chen, Z.H.; Ma, C.F.; Zhou, Y.; Chen, J.; et al. Direct reduction of oxidized iron ore pellets using biomass syngas as the reducer. *Fuel Process. Technol.* **2016**, *148*, 276–281. [[CrossRef](#)]
12. Yang, Y.R.; Guo, L.; Guo, Z.C. Numerical analysis of gasification characteristics in combined coal gasification and flash ironmaking process. *Appl. Therm. Eng.* **2020**, *171*, 115067. [[CrossRef](#)]
13. Spreitzer, D.; Schenk, J. Reduction of Iron Oxides with Hydrogen—A Review. *Steel Res. Int.* **2019**, *90*, 1900108. [[CrossRef](#)]
14. Sun, G.; Li, B.; Guo, H.J.; Yang, W.S.; Li, S.Y.; Guo, J. Thermodynamic study on reduction of iron oxides by H₂ + CO + CH₄ + N₂ mixture at 900 °C. *Energies* **2020**, *13*, 5053. [[CrossRef](#)]
15. Piotrowski, K.; Mondal, K.; Lorethova, H.; Stonawski, L.; Szymański, T.; Wiltowski, T. Effect of gas composition on the kinetics of iron oxide reduction in a hydrogen production process. *Int. J. Hydrog. Energy* **2005**, *30*, 1543–1554. [[CrossRef](#)]
16. Monazam, E.R.; Breault, R.W.; Siriwardane, R. Reduction of hematite (Fe₂O₃) to wüstite (FeO) by carbon monoxide (CO) for chemical looping combustion. *Chem. Eng. J.* **2014**, *242*, 204–210. [[CrossRef](#)]
17. Bohn, C.D.; Cleeton, J.P.; Müller, C.R.; Davidson, J.F.; Hayhurst, A.N.; Scott, S.A.; Dennis, J.S. The kinetics of the reduction of iron oxide by carbon monoxide mixed with carbon dioxide. *AIChE J.* **2010**, *56*, 1016–1029. [[CrossRef](#)]
18. He, S.Y.; Sun, H.Y.; Hu, C.Q.; Li, J.; Zhu, Q.S.; Li, H.Z. Direct reduction of fine iron ore concentrate in a conical fluidized bed. *Powder Technol.* **2017**, *313*, 161–168. [[CrossRef](#)]
19. Choi, M.E.; Sohn, H.Y. Development of green suspension ironmaking technology based on hydrogen reduction of iron oxide concentrate: Rate measurements. *Ironmak. Steelmak.* **2010**, *37*, 81–88. [[CrossRef](#)]
20. Zhang, T.; Lei, C.; Zhu, Q.S. Reduction of fine iron ore via a two-step fluidized bed direct reduction process. *Powder Technol.* **2014**, *254*, 1–11. [[CrossRef](#)]
21. Yi, L.; Huang, Z.C.; Jiang, T. Sticking of iron ore pellets during reduction with hydrogen and carbon monoxide mixtures: Behavior and mechanism. *Powder Technol.* **2013**, *235*, 1001–1007. [[CrossRef](#)]
22. Fan, D.Q.; Mohassab, Y.; Elzohiery, M.; Sohn, H.Y. Analysis of the hydrogen reduction rate of magnetite concentrate particles in a drop tube reactor through CFD modeling. *Metall. Mater. Trans. B* **2016**, *47*, 1669–1680. [[CrossRef](#)]
23. Fan, D.Q.; Sohn, H.Y.; Mohassab, Y.; Elzohiery, M. Computational fluid dynamics simulation of the hydrogen reduction of magnetite concentrate in a laboratory flash reactor. *Metall. Mater. Trans. B* **2016**, *47*, 3489–3500. [[CrossRef](#)]
24. De Faria, D.L.A.; Venâncio Silva, S.; de Oliveira, M. Raman microspectroscopy of some iron oxides and oxyhydroxides. *J. Raman Spectrosc.* **1997**, *28*, 873–878. [[CrossRef](#)]
25. Thibaud, R.J.; Brown, C.W.; Heidersbach, R.H. Raman spectra of possible corrosion products of iron. *Appl. Spectrosc.* **1978**, *32*, 532–535. [[CrossRef](#)]
26. Chen, H.S.; Zheng, Z.; Shi, W.Y. Investigation on the kinetics of iron ore fines reduction by CO in a micro-fluidized bed. *Procedia Eng.* **2015**, *102*, 1726–1735. [[CrossRef](#)]
27. Tiernan, J.M.; Barnes, P.A.; Parkes, G.M.B. Reduction of iron oxide catalysts: The investigation of kinetic parameters using rate perturbation and linear heating thermoanalytical techniques. *J. Phys. Chem. B* **2001**, *105*, 220–228. [[CrossRef](#)]
28. Pourghahramani, P.; Forssberg, E. Reduction kinetics of mechanically activated hematite concentrate with hydrogen gas using nonisothermal methods. *Thermochim. Acta* **2007**, *454*, 69–77. [[CrossRef](#)]
29. Chen, H.S.; Zheng, Z.; Chen, Z.W.; Yu, W.Z.; Yue, J.R. Multistep reduction kinetics of fine iron ore powder with carbon monoxide in a micro fluidized bed reaction analyzer. *Metall. Mater. Trans. B* **2017**, *48*, 841–852. [[CrossRef](#)]
30. Piotrowski, K.; Mondal, K.; Wiltowski, T.; Rizeg, G. Topochemical approach of kinetics of the reduction of hematite to wüstite. *Chem. Eng. J.* **2007**, *131*, 73–82. [[CrossRef](#)]
31. Fan, D.Q.; Elzohiery, M.; Mohassab, Y.; Sohn, H.Y. The kinetics of carbon monoxide reduction of magnetite concentrate particles through CFD modelling. *Ironmak. Steelmak.* **2021**, *48*, 1–10.
32. Jozwiak, W.K.; Kaczmarek, E.; Maniecki, T.P.; Maniukiewicz, W. Reduction behavior of iron oxides in hydrogen and carbon monoxide atmospheres. *Appl. Catal. A Gen.* **2007**, *326*, 17–27. [[CrossRef](#)]